Quantitative Evaluation of Short-Term Resting-State Brain Networks for Primary Insomnia Diagnosis

Chi Zhang[1, 2, *], Lina Sun[3], Shuang Ge[4], Yi Chang[5, *], Mingyan Jin[2], Yang Xiao[2], Hanbing Gao[2], Lin Wang[6], and Fengyu Cong[2, 3]

[1] Oncology department, Affiliated Zhongshan hospital of Dalian University, Dalian, Liaoning, China; chizhang@dlut.edu.cn (C.Z.)

[2] School of Biomedical Engineering, Faculty of Electronic Information and Electrical Engineering, Dalian University of Technology, China; jinmydlut@foxmail.com (M.J.); xiaoyang0318@foxmail.com(Y.X.); hanbing.gao@foxmail.com (H.G.); cong@dlut.edu.cn (F.C.)

[3] Faculty of Information Technology, Unniversity of Jyvaskyla, Finland; lnsun@dlut.edu.cn (L.S.)

[4] Shenzhen International Graduate School, Tsinghua University, China; ges20@mails.tsinghua.edu.cn (S.G.)

[5] Department of Neurology and Psychiatry, First Affiliated Hospital of Dalian Medical University, China; changee99@gmail.com (Y.C.)

[6] Department of Mechanical Engineering, Shenyang Institute of Engineering, China; wllgj373@sina.com (L.W.)

* Correspondence: chizhang@dlut.edu.cn (C.Z.); changee99@gmail.com

Chi Zhang, Lina Sun, and Shuang Ge have contributed equally to this work

Abstract:

Primary insomnia (PI) manifesting as insufficient and non-restorative sleep disturbs the function of central nervous system. Electroencephalogram (EEG), as a technique of recording the electrical signals of the brain, has demonstrated potential to access and quantify PI. However, most existing EEG indices rely on time-frequency analysis and separate channels, which limits its clinical application. In this study, we propose a novel quantitative evaluation method by introducing spatial information from resting-state brain networks of insomniacs to make rapid diagnosis implementable. To suppress false positive observations of coupling attributed to signal spread, the connections were binarized based on an adaptive threshold technology so that the statistical network characteristics were extracted automatically to form a comprehensive measurement index. The clinical experiments proved that the specificity of PI brain networks could be quantified objectively by the comprehensive index in the resting state. PI specificity showed consistency across the connectivity estimated in time (Pearson Correlation Coefficient, PCC), phase (Phase Lag Index, PLI) and frequency (Granger Causality, GC) domains. All the three kinds of connectivity revealed the significant difference between the PI patients and normal subjects (PCC: p=0.0021, PLI: p=0.0071, GC: p=0.0142). The strong connectivity of PI consistent with clinical rating scale indicates the hyperarousal of PI brain. It is difficult to achieve normal inhibition, so it consumes more resources in the resting state. An implication of this finding is that early clinical diagnosis of insomnia may be possible.

Keywords: Insomnia; EEG; Connectivity; Functional brain network; Causal brain network

1. Introduction

At present, about a third of the world population has experienced symptoms of primary insomnia (PI). Approximately 10% to 18% people suffer from insomnia that meets diagnostic criteria. Most of them have difficulties in getting to sleep, maintaining sleep or returning to sleep, and are often accompanied by the phenomenon of insufficient energy during the day [1].

Sleep quality is closely related to human health, life quality and work efficiency. In recent years, there has been growing recognition of the direct links between many mental illnesses and poor daytime alertness or insomnia. About pathophysiology, insomnia is associated with cognitive and physiological hyperarousal. A meta-analysis has shown that insomnia increases the risk of psychopathology arising [2]. The study of the physiological mechanism of insomnia plays a crucial role in the pathogenesis and diagnosis of mental diseases.

Insomnia was first studied in the 1880s, when its causes were largely understood from aetiology. However, the aetiological research failed to clarify what "conditioned arousal" was for chronic insomnia. Then, some researchers tried to explain the causes of chronic insomnia in terms of physical arousal (heart rate, breathing rate, myoelectric, urinary catecholamine, sympathetic nervous system) and cognitive arousal (excessive meditation) [3]. The extent to which these different forms of arousal contribute to insomnia remain poorly understood.

Previous works of the spectral correlation suggested that insomniacs might exhibit a third form of arousal: central nervous system arousal [4, 5]. Finding the right way to explore the brain structure, functional characteristics and internal mechanism of brain would contribute to the understanding of physiological and pathological mechanisms of primary insomnia. It was also expected to explain some psychiatric (anxiety, depression, etc.) or neurological (epilepsy, Alzheimer, etc.) symptoms and mechanisms, eventually benefitting human health.

Recent studies have reported differences in electroencephalogram (EEG) characteristics among insomnia patients with different clinical manifestations, so as to explain the pathogenesis of some psychiatric diseases with insomnia, or explain some behaviors (e.g. anxiety in the daytime) and propose appropriate treatment methods [6-8]. EEG has been used to investigate the relationship between subjective poor sleep quality and objective EEG recordings. Maria Corsi-Cabrera et al. [9] studied wakefulness EEG activity of PI patients the night before and the morning after they fell asleep, seeking out the reasons for excessive arousal in the morning and inability to return to sleep. They found the control subjects exhibited significantly decreased Beta and Gamma power during post-sleep, whereas there was no change from pre-sleep to post-sleep in the PI group. A large number of studies have also demonstrated that elevated Beta wave activity may be associated with high cortical arousal in patients, resulting in decreased sleep quality and even insomnia [5]. Spiegelhalder et al. [10] analyzed the high-frequency EEG power of PI patients in different sleep stages (NREM and REM) and reported their increased power values in the EEG Beta range during NREM stage 2 sleep but not during REM sleep in comparison to good sleeper controls. Freedman et al. [11] found absolute EEG Beta power increased during wake, stage 1 and REM sleep but not during NREM stages 2–4. Perlis et al. [12] described increased Beta power of PI in both REM and NREM sleep. Since findings in PI sleep are inconsistent, this aspect of increased high frequency power in PI patients remains to be further elucidated.

As a technological advancement in neuroscience, brain network analysis, measuring connectivity among different brain regions, can provide richer information about brain function state than simpler univariate approaches [13-16]. Brain network is a typical complex network, which can be divided into structural brain network, functional brain network and causal brain network from the perspective of network topology and network dynamics. Among them, structural brain network mainly reflects the physical structure of the brain, relying on neuroimaging techniques, such as MRI and Diffusion Tensor Imaging (DTI). Functional brain network reflects the statistical connections among the nodes of different brain areas, and the causal brain networks represent the information flow and information interaction among the nodes. EEG, Magnetoencephalography (MEG), fMRI and other imaging modalities enable the construction of functional brain networks and causal brain networks [17, 18]. Millisecond time resolution of EEG in the brain connectivity has significant advantages, which is helpful to define the causality of brain connectivity and to provide short time window for information exchange [19].

Recently, the research of functional brain networks has made a lot of progress in insomnia. Killgore et al. [20] tested the sensorimotor network of patients with sleep disorders and found that difficulty in sleeping was related to the enhanced functional connections between the primary visual cortex and other sensory regions (such as the primary auditory cortex,

smell cortex and auxiliary motor areas). Chen et al. [21] studied the internal relationship between significant networks and emotional regions in insomniacs, and found that functional connections between insula and significant networks were enhanced in these patients. In addition, enhanced functional connections between insula and emotional circuits (cingulate cortex, thalamus, and precuneus) were observed in PI [22]. These findings have shown that PI can affect different regional multi-nerve coordination. Taken together, PI may not only affect local functional systems, but also cause global disorder. However, the quantitative analysis of whole-brain connectivity is still lacking. In addition, choosing different connectivity-estimated methods to construct brain networks may get different results. Common methods of connectivity estimation include temporal correlation, synchronous likelihood estimation and phase-based calculation. Temporal correlation represents an empirical characterization of the temporal relationship between regions, without indicating how the temporal covariation is mediated. It is simple, fast and most commonly used measure [23]. Nevertheless, previous studies have shown that correlation, coherence, amplitude envelope correlation suffer from the primary and secondary leakage. Therefore, imaginary coherency [24] and Phase Lag Index (PLI) [25] were developed to address the problem. In the phase-based estimations, the signals are orthogonalized with respect to each other to remove zero-lag mixing prior to computing the correlation between the amplitudes. These interaction estimations are insensitive to leakage, whereas one important and frequently overlooked limitation is that spurious interactions may arise as an unwanted by-product of a truly interacting pair of sources [26].

With the development of brain network research and the progress of neuroimaging, it has been illustrated that the mutual influence between each pair of nodes is not completely equal, it may be directional with the flow of information among network nodes. As a special functional brain network, the causal brain network is generally constructed based on the theory of causality. It provides a directed network perspective and demonstrates a spontaneous information flow and causal influence between distinct brain regions, which provides insight into our understanding of the brain functional architecture [27-29]. Yan et al. [27] found the causality-based functional directed network was stable and reproducible in the young population. Nonetheless, previous studies did not account for causal interactions among resting-state brain networks in the PI patients [30]. The resting-state is defined as a baseline state of brain activity when a person is resting quietly but awake without performing any task [31]. Our hypothesis is that the brain networks of PI patients are different from healthy individuals in the resting state, which can be evaluated quantitatively.

In this context, we propose an EEG-based quantitative analysis method of PI whole-brain connectivity in the resting state. In order to demonstrate the versatility and stability of the method, the connectivity is estimated in three domains (i.e. time, phase, and frequency) to construct functional and causal brain networks. In time domain, the correlation analysis is realized by Pearson Correlation Coefficient (PCC) between the EEG time-series. In phase domain, the connectivity is measured by PLI to reduce leakage issue rising up during instantaneous signal spread. In frequency domain, Granger Causality (GC) based on Partial Directed Coherence (PDC) is calculated to perform causal analysis of EEG to construct directed network. Then, the connectivity matrices are binarized by an adaptive threshold technology to further remove spurious interactions. It selects the set of edges that together form the connected graph on which network organization is evaluated by clustering coefficient, characteristic path length, and global efficiency. These statistical network characteristics constitute a comprehensive measurement index. Finally, statistical analysis is performed to verify whether the proposed method is able to distinguish between PI and healthy control and assessed the functional and causal connectivity of PI.

This paper is organized as follows. In Section 2, we describe the experimental details and EEG data preprocessing (see Section 2.1 and 2.2), illustrate traditional time-frequency analysis of resting-state EEG from PI patients (see Section 2.3), elaborate the connectivity analysis in time, phase, and frequency domain to construct functional and causal brain networks (see Section 2.4, 2.5, and 2.6), and discuss the quantification method based on the network characteristics (see Section 2.7 and 2.8). Results of the study are presented in Section 3 and discussed in Section 4. Finally, the paper concludes in Section 5.

2. Materials and Methods

2.1. Experiments and data

Studies have shown that PI is different from those who also suffer from mental disorder synchronously. It affects interregional neural coordination of multiple interacting functional brain networks [32]. Therefore, patients with insomnia symptoms only were selected as the experimental subjects. None of the subjects reported neurological or developmental disorders.

This study was reviewed and approved by Ethics Committee, the First Affiliated Hospital of Dalian Medical University. Written informed consents were obtained from all participants before the experiments. Twenty-eight subjects aged from 20 to 65 years (mean age, 43.86 years) were recruited in the hospital. They were divided into PI and control groups according to the clinical selection criteria with fourteen subjects (9 females) in each group.

PI was diagnosed by the doctors in the hospital. They ruled out that the insomnia was caused by other disorders, e.g. mental disorders, based on medical examinations. At the same time, PI fulfilled the following criteria: (1) meet the criteria for diagnosis of insomnia in Diagnostic and Statistical Manual of mental disorders-fifth edition (DSM-5; American Psychiatric Association, 2013), (2) a score $\geqslant 7$ on the Pittsburgh Sleep Quality Index (PSQI), (3) a score $\geqslant 8$ on the Insomnia Severity Index (ISI), (4) do not meet the criteria for diagnosis of mental disorders other than insomnia confirmed by Structured Clinical Interview for DSM-IV Axis I Disorders (SCID-I). Healthy control met the following criteria: (1) have no complaints of sleep disturbance or daytime symptoms attributable to unsatisfactory sleep; (2) no report of sleep disruption due to a substance (e.g. drug, alcohol, caffeine, or nicotine) use, abuse, or withdrawal; (3) a score < 5 on PSQI, (4) a score < 8 on ISI, (5) no diagnosis of mental disorders by SCID-I [33].

Table 1 shows statistical data and clinical characteristics of all participants (mean value ± standard error). The control and PI groups reveal no significant differences between group in age (p=0.9369) and education (p=0.1808). The average illness duration for participants in the PI group is 5.29 years. The patients with PI have significantly higher PSQI and ISI scores than the controls ($p < 0.001$).

Participants sat on a comfortable chair during EEG measurement. Sixty standard electrodes (see Fig.1) were attached to the scalps following the International 10-20 System to collect the resting EEG data of PI and control groups for about 10 minutes. All the subjects were awake without any drowsy feeling report before the experiments. In order to achieve the rapid evaluation of PI, the first 20-second EEG were selected in data analysis. The EEG sampling frequency was 500Hz. The data of the two groups were collected in the same periods of the daytime (9:00~12:00 and 13:30~17:00) to exclude the influence of time factor.

Table 1. Statistical data and clinical characteristics of all participants.

Parameter	Primary insomnia	Healthy control	p value
Age (years)	44.00 ± 3.50	43.71 ± 4.95	0.9369
Gender	9 females, 5 males	9 females, 5 males	
Education (years)	10.00 ± 1.37	13.14 ± 1.75	0.1808
Illness duration(years)	5.29 ± 1.97		
PSQI	16.10 ± 1.27	3.57 ± 0.61	**<0.001**
ISI	21.20 ± 1.80	2.57 ± 0.48	**<0.001**

PSQI, Pittsburgh Sleep Quality Index; ISI, Insomnia Severity Index. Means ± standard deviations of age, education, illness duration, PSQI, and ISI were reported in the original units. With unpaired two-sample t-test, only PSQI and ISI reveal statistical differences (p<0.001) between the two group.

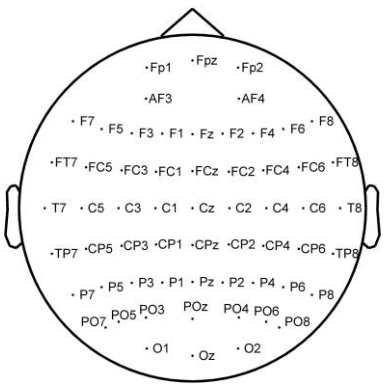

Fig. 1 Distribution of EEG electrodes. Sixty standard electrodes are arranged in accordance with the International 10-20 System to collect the EEG data.

2.2. Data preprocessing

In the clinical environment, the raw EEG signals are inevitably interfered by artifacts such as power frequency (50Hz), muscle movement, and blinking. To reduce the noises preliminarily, the original signals were filtered through a 0.5-50Hz bandpass filter and 50Hz notch filter.

Since previous studies have demonstrated the high correlation between Beta activity and insomnia [4, 9, 10, 34], the preprocessed signals were further processed by discrete wavelet transform (DWT) with fourth order Daubechies wavelet and four level decomposition to obtain the sub-band EEG waves (i.e. Beta) to perform functional brain network analysis. DWT is an effective method to analyze various components (e.g. approximate and detailed components) of EEG due to its attractive properties such as good local representation in both time and frequency domain and multi-rate filtering [35]. On the basis of DWT, the wavelet-based threshold technique in [36-39] was applied to correct the sub-band EEG waves further.

The comparison of the EEG signals before and after preprocessing is shown in Fig. 2. Fig. 2(a) gives a typical 4-second original EEG signal disturbed by a variety of artifacts. Fig. 2(b) shows Beta waves extracted by wavelet decomposition. The relatively large fluctuations which may be caused by body movements were apparently eliminated, whereas a few of artifacts are still left (e.g. the artifacts probably caused by blinks in the red boxes). These artifacts are removed in Fig. 2(c). Compared to the original signal, the corrected signal in Fig. 2(c) presents more detailed components and retains the main trend.

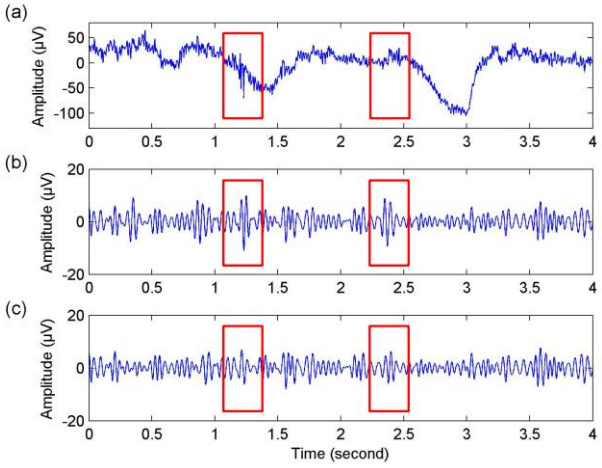

Fig. 2. EEG data preprocessing. (a) Original EEG signal. (b) Extracted Beta waves. DWT with Daubechies wavelet is performed to obtain the Beta waves. (c) Artifact removal. Wavelet-based threshold technique in [36-39] is utilized to removed the residual artifacts.

2.3. Time-frequency analysis

Time-frequency analysis has been widely used in the sleep research of the patients with insomnia. Through time-frequency analysis, the frequency components of EEG in each time period can be intuitively compared between normal and patient groups, which is conducive to subsequent analysis. Short-time Fourier transform and wavelet transform are two common algorithms in the time-frequency analysis [40]. Since wavelet transform has the advantage of good local representation in both time and frequency domains compared to Fourier transform, it is more adapted to the time-frequency analysis of non-stationary signals. Wavelet transform was adopted in time-frequency analysis.

For a time series $x(t)$ with length T (t=0, 1, 2, ..., T-1), wavelet coefficient at time t_0 is estimated by the formula

$$WT_x(a,t_0)=\frac{1}{\sqrt{|a|}}\sum_{t=0}^{T-1}x(t)\cdot\psi\left(\frac{t-t_0}{a}\right), \quad (1)$$

where a and t_0 represent scaling and shifting parameters, respectively. ψ denotes mother wavelet. In this study, the common-used Morlet wavelet was employed as mother wavelet [40]. Morlet wavelet is defined as

$$\psi(t, f_c) = \frac{1}{\sqrt{\pi\sigma^2}} e^{i2\pi t f_c} \cdot e^{\frac{-t^2}{2\sigma^2}}, \quad (2)$$

where σ and f_c are the bandwidth and center frequency of Morlet wavelet. It follows Gaussian distribution in time and frequency domain around f_c. Scaling parameter a is correlated with frequency f.

$$f = \frac{f_s \cdot f_c}{a} \quad (3)$$

where f_s is the sampling frequency of $x(t)$. The wavelet time-frequency (WTF) spectrum $WT(t, f)$ can be obtained through Eqs. (1)-(3). The preprocessed signals with the frequency range of 0.5-50Hz was used as the input time series $x(t)$. $|WT(t, f)|^2$ represent the power values of EEG data varying with time t and frequency f.

2.4. Connectivity Estimation Based on Pearson Correlation Coefficient

According to graph theory, a brain network can be represented by a graph G(**N**, **E**) where **N** and **E** are the node and edge (or link) sets. We assigned EEG electrodes to the nodes of the brain networks. The adjacency relations among the nodes in the networks can be described by the adjacency matrix ***A*** whose element ***A***(i, j) shows the measured edge between electrodes (nodes) i and j. Since the EEG electrodes are distributed in different brain regions, the edges embody functional connectivity among these brain regions. As mentioned above, different connectivity-estimated methods may affect the the quantitative analysis of whole-brain connectivity. Thus, PCC, PLI, GC and PDC were used to estimate the connectivity so that the quantitative analysis had a certain generalization ability.

In time domain, a simple and commonly used measure of the functional connectivity is the correlation coefficien [23]. If $x(t)$ and $y(t)$ are the EEG time series from nodes i and j, the correlation between them can be expressed as

$$r_{ij} = \frac{\sum_{k=1}^{n}(x_k - \bar{x})(y_k - \bar{y})}{\sqrt{\sum_{k=1}^{n}(x_k - \bar{x})^2 \sum_{k=1}^{n}(y_k - \bar{y})^2}}, \quad (4)$$

where r_{ij} is Pearson correlation coefficient. x_k and y_k correspond to the signal amplitudes at kth moment. n is the sample number of $x(t)$ and $y(t)$. The correlation coefficient is the covariance of the two samples divided by the multiplication of the standard deviation. Covariance reflects the relevancy between two random variables. If a variable varies with another variable at the same time, then the covariance of the two variables is positive, otherwise the covariance is negative. Nevertheless, if the points are distributed discretely, covariance value may be large, which is difficult to reflect the reality relevancy of the two variables, as relevancy is also related to the dispersion of the variables themselves. PCC is provided to solve this problem. An important mathematical characteristic of PCC is that changes in the position and scale of the two variables will not cause the coefficient to change.

Here, the extracted Beta waves were taken as the time-varying signals. For rapid assessment of PI in the resting state, we employed a sliding window with the length to be one second to analyze Beta oscillation data within 20 seconds. In the sliding window, the correlation coefficient between two channel Beta waves was considered as the element of the adjacency matrix to construct the brain networks.

2.5. Connectivity Estimation Based on Phase Lag Index

PLI reflects the consistency of the phase lead or lag of two leads from the perspective of phase. The PLI value between EEG signals from nodes i and j can be calculated by the following equation

$$PLI_{ij} = \left|\left\langle sign[\Delta\varphi(t_k)]\right\rangle\right|, \quad (5)$$

where $\Delta\varphi(t_k)$ is the instantaneous phase difference between the two leads at the moment k. *sign* denotes a symbolic function. $< \bullet >$ refers to averaging in the time domain. When $\Delta\varphi(t_k) > 0$, $sign[\Delta\varphi(t_k)]=1$. It means that the phase of

the two leads is synchronous. If $\Delta\varphi(t_k) < 0$, $sign[\Delta\varphi(t_k)]$=-1. It reveals that the phase of the two leads is out of synchronization. Thus, PLI values lie in the range from 0 to 1. The larger the PLI values are, the stronger the phase coupling is.

2.6. Connectivity Estimation Based on Granger Causality

Different from the previous two methods, in this section, we constructed causal brain networks using GC to supplement the brain networks. In the causal brain networks, the connections between nodes are directional, reflecting the direction of the information flow. GC model does not require a priori assumption of the interactions between brain regions. Its concept is proposed by Wiener. Its algorithm is realized by Granger through the linear regression model of random process [41].

GC is based on predictability and precedence. Simply put, Granger causality is a vector-valued stochastic process that assumes two vectors such as $X = X_1, X_2, \cdots X_n$ and $Y = Y_1, Y_2, \cdots Y_m$ have common distributions. If *Y* depends not only on its past but also on the past of *X*, i.e. the past of *X* contains information that can help predict the future of *Y*, then we can say that *Y* G-causes *X* or *X* is a cause of *Y*, and the two vectors have a causal relationship [42].

Since GC model requires the data to be covariance-stationary, whether Granger causality is adapted to the brain network analysis needs to be tested. Hence, we calculated autocorrelation function of the preprocessed EEG time series. As shown in Fig. 3, the autocorrelation function first rises, then falls, and finally converges to 0. It conforms to the law that a stationary time series generally fluctuates around its mean. Further, Augmented Dickey Fuller (ADF) test was utilized to confirm the stationarity of the preprocessed EEG. ADF test results showed that the current data had no unit root. It rejected the null hypothesis (unit root existed), so the preprocessed EEG was considered to be covariance stationary.

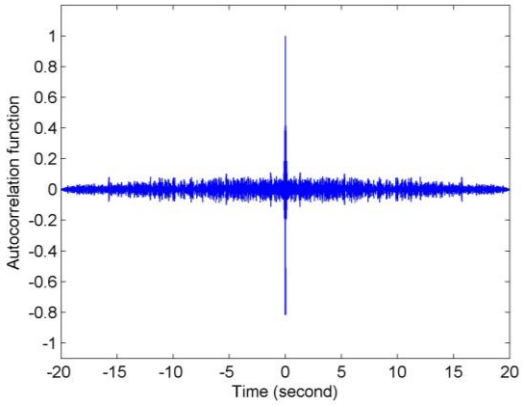

Fig. 3. Self-correlation test. The autocorrelation function of the preprocessed EEG data fluctuates around 0 and finally converges to 0.

Finally, based on Multivariate Autoregressive (MVAR) Model and PDC analysis, Granger causality was successfully applied to the analysis of brain networks. The PDC based on MVAR model quantified the direct causality among nodes, effectively avoiding pseudo causality [43].

Consider the EEG signals of *N* channels at time *t*

$$U_t = [U_{1t}, U_{2t}, \cdots, U_{it}, \cdots, U_{Nt}]^T \tag{6}$$

where U_{it} represents the time series of the channel *i*. The *p*th MVAR model can be expressed as

$$U_t = \sum_{k=1}^{p} A(k) U_{t-k} + E(t) \tag{7}$$

where $A(k)$ denotes the model coefficient matrix of *N* by *N*. $E(t)$ stands for random noise. The key parameter of MVAR model is the order *p*. It represents that the sequence at the current moment *t* is related to the sequence values at the *p* previous moments, or *p* past moments of the sequence predict the sequence of the current moment *t*. In this work, $A(k)$ was calculated with the GCCA (Granger Causal Connectivity Analysis) Toolbox [42]. *p* was determined by Akaike Information Criterion (AIC) and Bayesian Information Criterion (BIC).

Based on the MVAR model, PDC is one of the methods to find the Granger causality between any two channels at different frequencies [44]. In PDC, the coefficient matrix $A(k)$ of MVAR model was transformed as

$$\overline{A(f)} = I - \sum_{k=1}^{p} A(k) e^{-i2\pi fk} \tag{8}$$

where f represents the frequency.

Then, the element of $\overline{A(f)}$ in row i and column j can be expressed as

$$\overline{A_{i,j}(f)} = \begin{cases} 1 - \sum_{k=1}^{p} a_{i,j}(k) e^{-i2\pi fk}, & i = j \\ -\sum_{k=1}^{p} a_{i,j}(k) e^{-i2\pi fk}, & otherwise \end{cases} \tag{9}$$

At frequency f, the element of PDC in row i and column j is defined as

$$PDC_{i,j}(f) = \frac{\left|\overline{A_{i,j}(f)}\right|}{\sqrt{\bar{a}_j^{T}(f)\bar{a}_j^{T}(f)}} = \pi_{i,j}(f) \tag{10}$$

where $\bar{a}_j(f)$ is the jth column of $\overline{A_{i,j}(f)}$ (j = 1, 2, …, N). The average value of the $PDC_{ij}(f)$ is obtained by

$$\overline{PDC_{i,j}} = \frac{\sum_f \bar{\pi}_{i,j}(f)}{\nabla f} \tag{11}$$

where ∇f is the Beta band range of 13-30Hz. $\overline{PDC_{i,j}}$ denotes the direction and intensity of the information flow from channel j to channel i.

2.7. Binarization of adjacency matrix

In order to facilitate the feature extraction of the brain networks, the adjacency matrix was binarized based on an adaptive threshold technology. First, the diagonal elements of the adjacency matrix were set to zero to exclude self-connections of nodes. If the element $a_{i,j}$ of adjacency matrix exceeded a threshold T, it was set to 1, and to 0 otherwise. For the binarized adjacency matrix A, its element is expressed as

$$a_{i,j} = \begin{cases} 1, & i \neq j \wedge \rho_{i,j} \geq T(w), \\ 0, & \text{otherwise.} \end{cases} \tag{12}$$

where $T(w)$ represents the threshold in every window w. $a_{i,j}$ denotes the ith row and jth column element of A. $\rho_{i,j}$ is the correlation value estimated from Sections 2.4, 2.5 or 2.6.

Since the threshold defines the topology of the network, it is important to choose a proper threshold. In order to characterize the dynamics of global network, the highest possible threshold was selected for each time window to reduce the randomness of the network and avoid the appearance of isolated nodes. Starting from a threshold $T(w)$=1, we gradually reduced the threshold. At each step, the second smallest eigenvalue $\lambda_{\min}$ of the corresponding Laplace matrix was computed. When the eigenvalue was greater than zero, the threshold $T(w)$ was determined to implement binarization so that the established network belongs to the connected graph [45]. According to [46], $\lambda_{\min}$ is positive if and only if the graph is connected. Laplace matrix L can be calculated by the following equation

$$L_{i,j} = k_i \delta_{i,j} - a_{i,j} \tag{13}$$

where k_i denotes the degree of ith node. $\delta_{i,j}$ is the Kronecker delta.

$$\delta_{i,j} = \begin{cases} 0, & i \neq j \\ 1, & i = j \end{cases} \tag{14}$$

2.8. Quantification and evaluation of brain network characteristics

To evaluate the characteristics of PI brain network, the clustering coefficient, characteristic path length, and global efficiency were integrated to form a comprehensive index.

The clustering coefficient of a node, C_i, is the ratio of the number of links that exist between the nearest neighbors of the chosen node and the number of possible links between them [15]. A large clustering coefficient means high local functional overlap of densely connected neighborhood elements. The equation of clustering coefficient can be expressed as

$$C_i = \frac{E_i}{k_i(k_i - 1)/2} \tag{15}$$

where E_i represents the number of edges connected between adjacent nodes of node i. k_i denotes the number of links between node i and all its neighboring nodes. The clustering coefficient of a network, C, is the average over the clustering coefficients of all nodes. By definition, the clustering coefficient values lies in the range from 0 to 1.

The characteristic path length L refers to the average value of the shortest path between all the node pairs. The shortest path length $d(i, j)$ is defined as the minimum number of links that must be traversed to go from node i to node j. Therefore, $d(i, j) \geq 1$. $d(i, j)=1$ if i and j are neighbors, whereas $d(i, j) \to \infty$ if the nodes are disconnected. It refects the functional dispersion of the node pairs in the network. The characteristic path length L was computed as below

$$L = \frac{1}{N(N-1)} \sum_{i \neq j \in V} d(i, j) \tag{16}$$

where $d(i, j)$ is the shortest path length. N denotes the number of all nodes in the network. V stands for the set of all nodes. Small characteristic path length L implies stronger potential for integration and higher information transmission efficiency.

Assuming a parallel information flux, the communication efficiency between two nodes is inversely proportional to the shortest path length. The efficiency of a set of nodes is the sum of the efficiencies of all node pairs, normalized by maximal number of links $N(N-1)/2$. When the node set (V) contains all nodes, the efficiency obtained from Eq. (17) is viewed as the global efficiency

$$E_{\text{global}} = \frac{1}{N(N-1)} \sum_{i \neq j \in V} \frac{1}{d(i, j)} \tag{17}$$

where $d(i, j)$ is the shortest path between the ith node and the jth node. N denotes the number of all nodes in the network. V stands for the set of all nodes.

Many recent studies have certificated that there exhibits "small-world" behavior in different scales of brain networks [47-49]. The "small-world" network has bigger clustering coefficient and smaller characteristic path length compared to a random network. Our hypothesis is that PI can cause the change of resting-state brain networks. Thus, it may be reflected in "small-world" related features.

Here, considering that global efficiency is inversely proportional to characteristic path length, the ratio of the product of global efficiency and clustering coefficient to characteristic path length is taken as the comprehensive index of network characteristics.

$$\eta(w) = \frac{E_{\text{global}}(w) \times C(w)}{L(w)} \tag{18}$$

where $E_{\text{global}}(w)$, $C(w)$, and $L(w)$ represent global efficiency, clustering coefficient, and characteristic path length in sliding window w. Large comprehensive index η implies strong "small-world" attributes.

2.9. Classification based on brain network characteristics

The classification of healthy status (normal or PI) about sleep was performed using a machine learning method of bidirectional long short-term memory (Bi-LSTM) network (see method details in [50]).

The LSTM structural properties of sharing weights based on gate mechanism allow it to learn the timing characteristics of the data, facilitating long-term memory. Compared to the classical unidirectional LSTM, the Bi-LSTM can capture the dynamic information from both earlier and later segments in EEG sequence [51].

As shown in Fig. 4, the classifier consists of four layers. The first layer takes the brain network characteristics as input. The second is the LSTM layer, which learn the long-term dependencies and compensate for the vanishing gradient. The third is a fully connected layer, which is used to integrate the features extracted by the LSTM layer. It is a linear combination of the output of all LSTM units during the last time step. The function of this layer combines different feature-dynamic

information learned from each LSTM unit. The output of this layer is set as the input of softmax function to predict the healthy status (normal or PI). The fourth is the output layer, producing the recognized healthy status category.

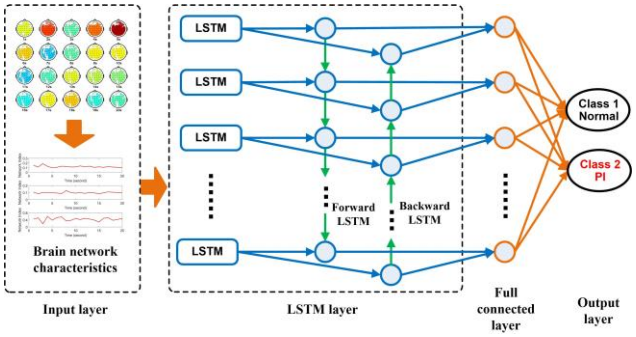

Fig. 4. Architecture of the Bi-LSTM classifier. The inputs of the classifier are the brain network characteristics. The output of the classifier is the healthy status category (normal or PI) about sleep.

In this paper, the brain network characteristics of each subject were estimated under three connectivity conditions (PCC, PLI, and GC) and the estimation was implemented in the resting state EEG of 20 seconds. Thus, the data of each subject is represented by a matrix of 3×20. The dataset of all subjects are set as the input of the Bi-LSTM classifier. It was divided into the training set and test set. Their ratio was 4:3.

To verify the evaluation effect of the brain network characteristics and expand the test set, the EEG of four additional subjects was collected. The data acquisition condition was the same as that in Section 2.1. All the four subjects are females. Two of the subjects are PI patients (age: 52 and 34, illness duration: 10 and 5 years). The other two subjects are normal individuals (age: 57 and 31). Their network characteristics were used for testing. Therefore, the test set was updated. It had 960 samples and accounted for 50%. The train set had 960 samples and accounted for 50%.

3. Results

3.1. Time-frequency analysis

Figs. 5 and 6 show the WTF diagrams of a healthy control and a PI patient respectively. Their display range is 0-50Hz. The Beta oscillation activities can be observed in both the WTF diagrams of the healthy control and PI patient. The distribution of Beta oscillations is different in the frontal and posterior regions. The PI's activation phenomenon around 20Hz in the posterior regions is more obvious. Hence, the power in Beta band was calculated and further statistical analysis of all subjects was performed.

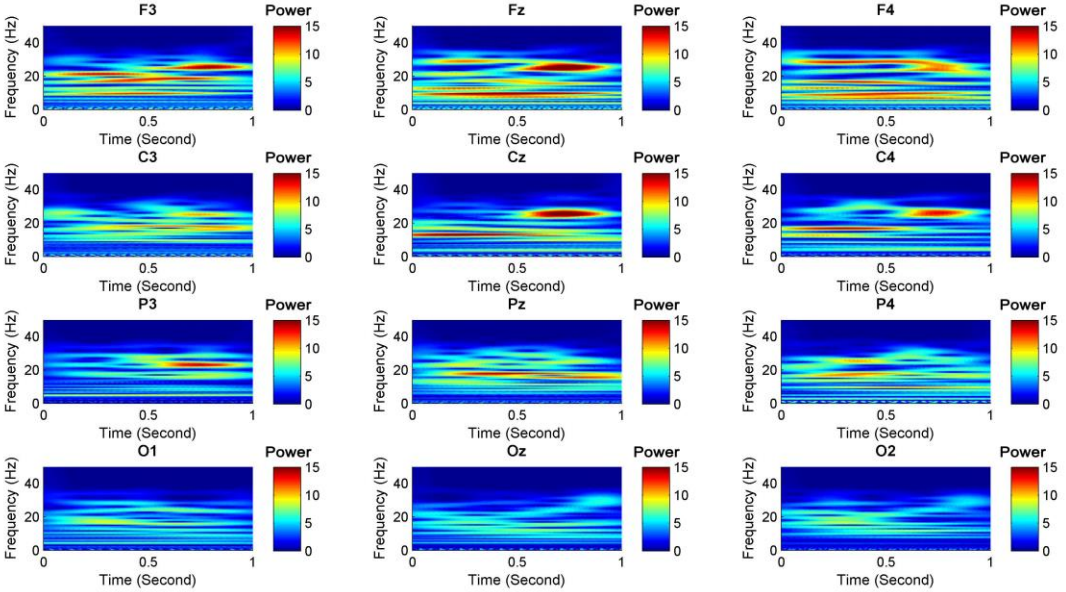

Fig. 5. Results of time frequency analysis for a healthy control. Electrodes F3, Fz, F4, C3, Cz, C4, P3, Pz, P4, O1, Oz, and O2 distributed in the whole brain are selected to demonstrate the WTF diagrams. Color bar indicates WTF power. Beta activity around 20Hz is relatively active throughout the entire brain.

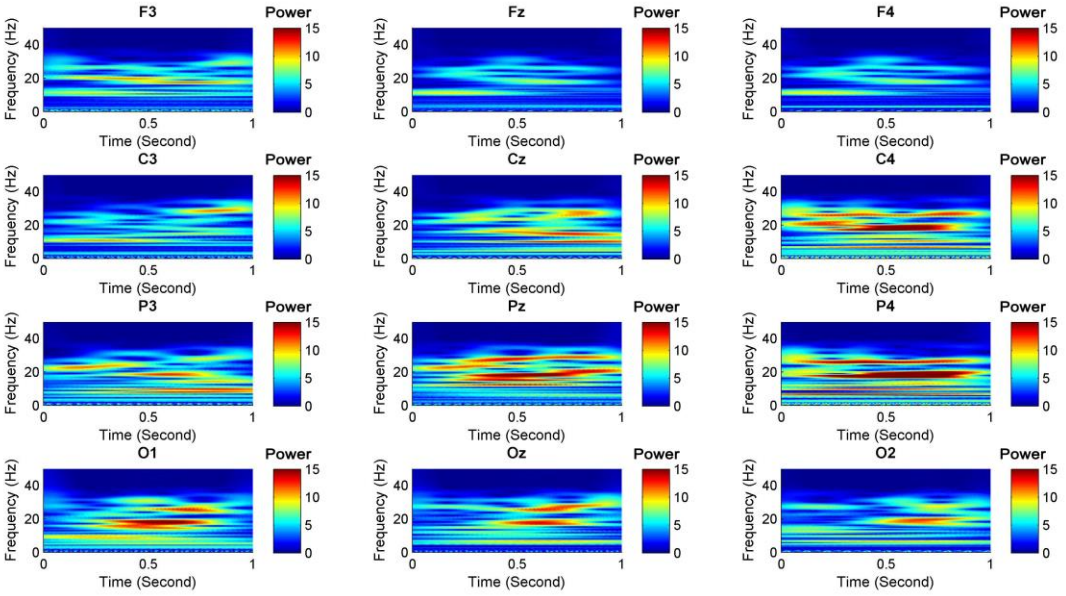

Fig. 6. Results of time frequency analysis for a PI patient. Electrodes F3, Fz, F4, C3, Cz, C4, P3, Pz, P4, O1, Oz, and O2 distributed in the whole brain are selected to demonstrate the WTF diagrams. Color bar indicates WTF power. Beta activity around 20Hz is relatively active throughout the entire brain.

Fig. 7 shows the brain topographies of Beta power. The occipital area of the PI patient is active. Compared to the healthy control, the Beta power of PI in occipital area is higher. It reveals the difference in the topographical distribution. Thus, the following statistical analysis for all the subjects was performed on the electrodes in different brain regions.

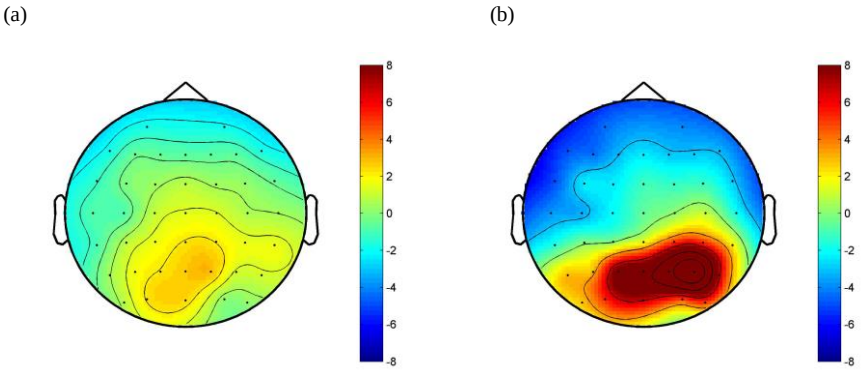

Fig. 7. Brain topographies of Beta power. (a) Brain topography of a healthy control. (b) Brain topography of a PI patient. All the sixty electrodes in Fig. 1 are used to demonstrate the topographies. The WTF power is converted to relative power by subtracting the average power of all the channels so that the image is centred around zero. Color bar indicates the relative power.

Fig. 8 shows the power in Beta band of the two groups. There are differences of Beta power averages between the two groups, but the differences only reflect in some frontal and posterior channels. The Beta power averages of the PI group in the specific channels are higher than those of the healthy control group.

Then, mixed two-way ANOVA was performed for Beta power with groups as the independent variable and derivations (frontal and posterior channels) as the within-subjects variables. As shown in Table 2, there is no significant difference of Beta power between the control and patient groups in frontal and posterior regions. It reveals large deviation among the subjects during resting state.

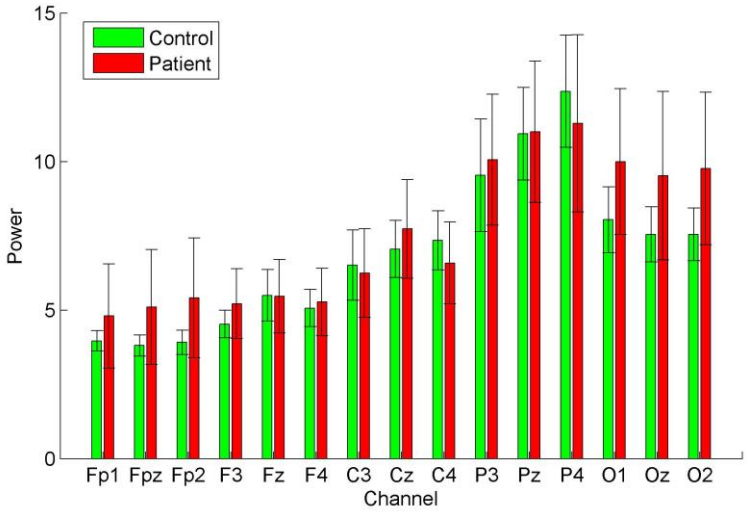

Fig. 8. Beta absolute power of normal group and patient group. The *x*-axis represents channel. The *y*-axis refers to the absolute power obtained by WTF where the frequency range corresponds to Beta band. The error bars are given in the form of mean ± standard deviation.

Table 2. ANOVA analysis: insignificant differences in Beta absolute power.

	Group		Derivation		Group by Derivation	
	F	*p*	*F*	*p*	*F*	*p*
Frontal regions	1.07	0.3024	0.23	0.9474	0.11	0.9892
Posterior regions	0.55	0.4594	0.74	0.5957	0.18	0.9696

Mixed Group × Derivation ANOVAs. Group: insomnia and control group; Derivation: channels; Frontal regions: Fp1, Fpz, Fp2, F3, Fz, and F4; Posterior regions: P3, Pz, P4, O1, Oz, and O2. The absolute power is obtained by WTF where the frequency range corresponds to Beta band.

3.2. Evaluation of functional brain Networks based on PCC

Fig. 9 shows the brain networks constructed by PCC during the resting state of 20 seconds. The number of connections for each network is indicated by the color within the color bar. Compared to the brain networks of healthy control (Fig. 9(a)), the most PI's networks have more links (Fig. 9(b)). The topological structure of the PI's networks is different from the healthy control. Additionally, the structure of the PI's networks is relatively stable throughout the 20-second resting process.

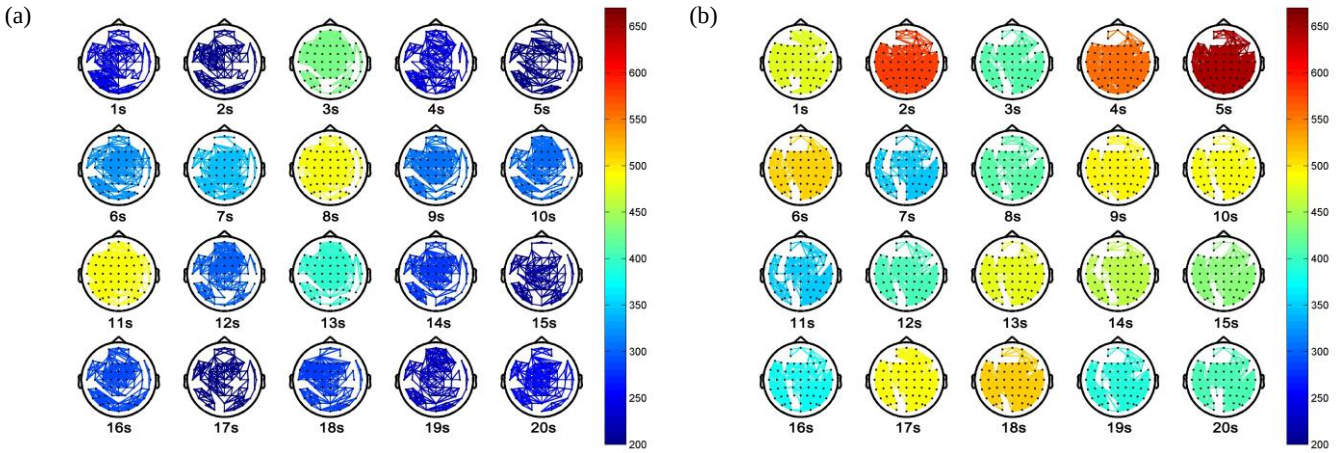

Fig. 9. Brain networks constructed by PCC in the resting state. (a) Healthy control. (b) PI patient. Color bar indicates link number. The EEG electrodes are assigned to the nodes of the brain networks. The connectivity is estimated by PCC and is binarized based on the adaptive threshold technology in Sec. 2.7. If there is a link between two nodes, it means the PCC value exceeds the threshold *T*.

Fig. 10 shows the statistical analysis results of characteristics of brain networks constructed by PCC. The blue and red lines represent the healthy control and PI groups respectively. The characteristic path length presents more obvious differentiation degree between groups (Fig. 10(b)), compared to the other two original network characteristics (Figs. 10(a) and (c)). Most the averages of characteristic path length of PI group are smaller than those of healthy control group. Through unpaired two-sample *t*-test, it reveals statistically significant differences of characteristic path length (p=0.0015**)** and insignificant differences of clustering coefficient (p=0.3938) and global efficiency (p=0.7042) between groups. It indicates that the characteristic path length of PI group is significantly shorter than that of healthy control group under the condition of PCC connectivity (p<0.01).

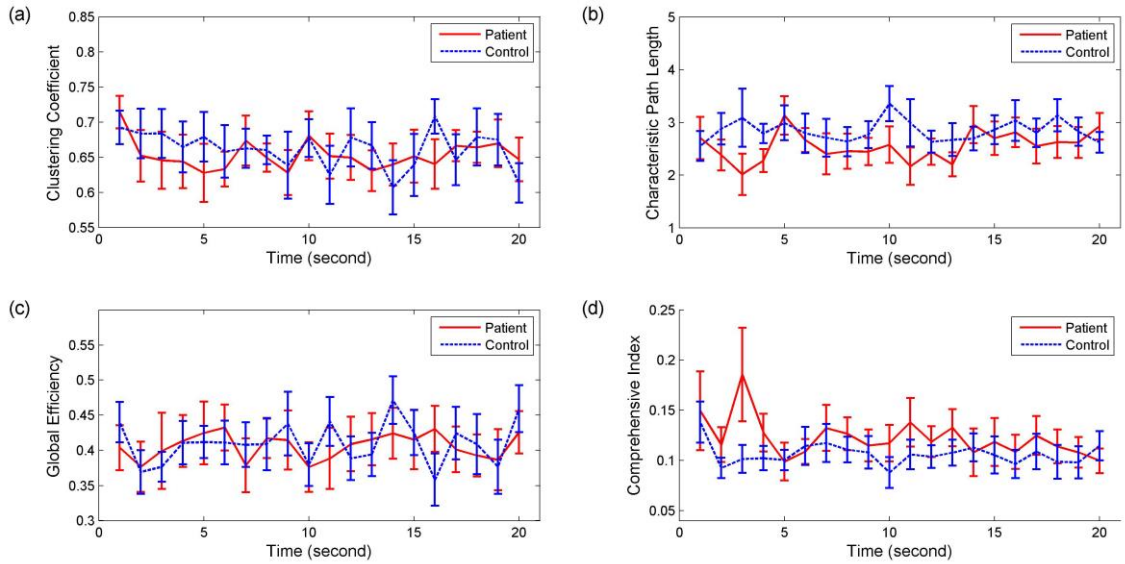

Fig. 10. Characteristics of brain networks constructed by PCC in the resting state. (a) Clustering coefficient. (b) Characteristic path length. (c) Global efficiency. (d) Comprehensive index. Clustering coefficient C, characteristic path length L, global efficiency E_{global}, and comprehensive index η are calculated by Eqs. (15)-(18) respectively. Their averages and standard errors are plotted. The error bars are given in the form of mean ± standard deviation.

Fig. 10(d) shows the proposed comprehensive index of network characteristics under the condition of PCC connectivity. The differentiation degree between groups is approximate to characteristic path length in Fig. 10(b). Most the comprehensive index averages of PI group are larger than those of healthy control group. Through unpaired two-sample t-test, it reveals statistically significant differences of comprehensive indices (p=0.0021**)** between groups**.** It indicates that the comprehensive index of PI group is significantly bigger than that of healthy control group under the condition of PCC connectivity (p<0.01).

3.3. Evaluation of functional brain Networks based on PLI

Fig. 11 shows Brain networks constructed by PLI during the resting state of 20 seconds. The PLI networks have wider range of link number variation than PCC networks. Compared to the healthy control (Fig. 11(a)), the PI patient has more dense connectivity in phase domain (Fig. 11(b)). There are also visual differences of topological structure in some networks, e.g. the 18th and 19th networks between the healthy control and PI patient.

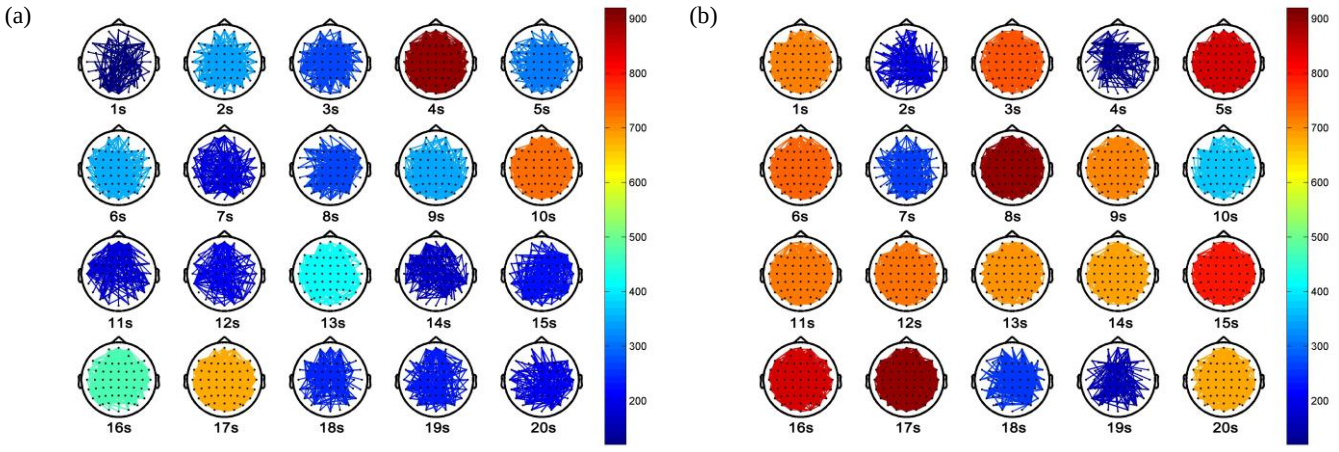

Fig. 11. Brain networks constructed by PLI in the resting state. (a) Healthy control. (b) PI patient. Color bar indicates link number. The EEG electrodes were assigned to the nodes of the brain networks. The connectivity was estimated by PLI and was binarized based on the adaptive threshold technology in Sec. 2.7. If there is a link between two nodes, it means the PLI value exceeds the threshold T.

Fig. 12 shows the statistical analysis results of characteristics of brain networks constructed by PLI. The blue and red lines represent the healthy control and PI groups respectively. The clustering coefficient (Fig. 12(a)) and global efficiency (Fig.

12(c)) present more obvious differentiation degree between groups in the original network characteristics (Figs. 12(a)-(c)). Most the averages of clustering coefficient and global efficiency of PI group are larger than those of healthy control group. Through unpaired two-sample *t*-test, it reveals statistically significant differences of clustering coefficient (*p*=0.0039**)** and global efficiency (*p*=0.0250) and insignificant differences of characteristic path length (*p*=0.0722) between groups. It indicates that the clustering coefficient (*p*<0.01) and global efficiency (*p*<0.05) of PI group are significantly larger than that of healthy control group under the condition of PLI connectivity.

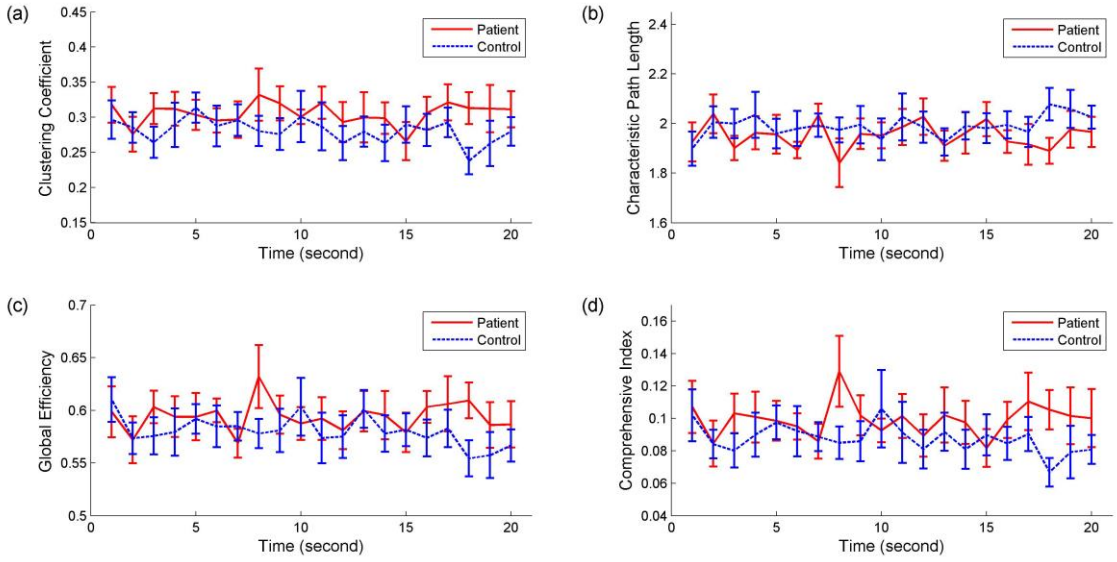

Fig. 12. Characteristics of brain networks constructed by PLI in the resting state. (a) Clustering coefficient. (b) Characteristic path length. (c) Global efficiency. (d) Comprehensive index. Clustering coefficient C, characteristic path length L, global efficiency E_{global}, and comprehensive index η are calculated by Eqs. (15)-(18) respectively. Their averages and standard errors are plotted. The error bars are given in the form of mean ± standard deviation.

Fig. 12(d) shows the proposed comprehensive index of network characteristics under the condition of PLI connectivity. The differentiation degree between groups is better than global efficiency in Fig. 12(c). Most the comprehensive index averages of PI group are larger than those of healthy control group. Through unpaired two-sample *t*-test, it reveals statistically significant differences of comprehensive indices (*p*=0.0071**)** between groups**.** It indicates that the comprehensive index of PI group is significantly bigger than that of healthy control group under the condition of PLI connectivity (*p*<0.01).

3.4. Evaluation of functional brain Networks based on GC

Fig. 13 shows Brain networks constructed by GC during the resting state of 20 seconds. Even though there are some fluctuations (e.g. the 1st, 7th, and 20th networks), most networks of the PI patient (Fig. 13(b)) also has more links than healthy control (Fig. 13(a)). Under the GC condition, the connectivity generally becomes denser.

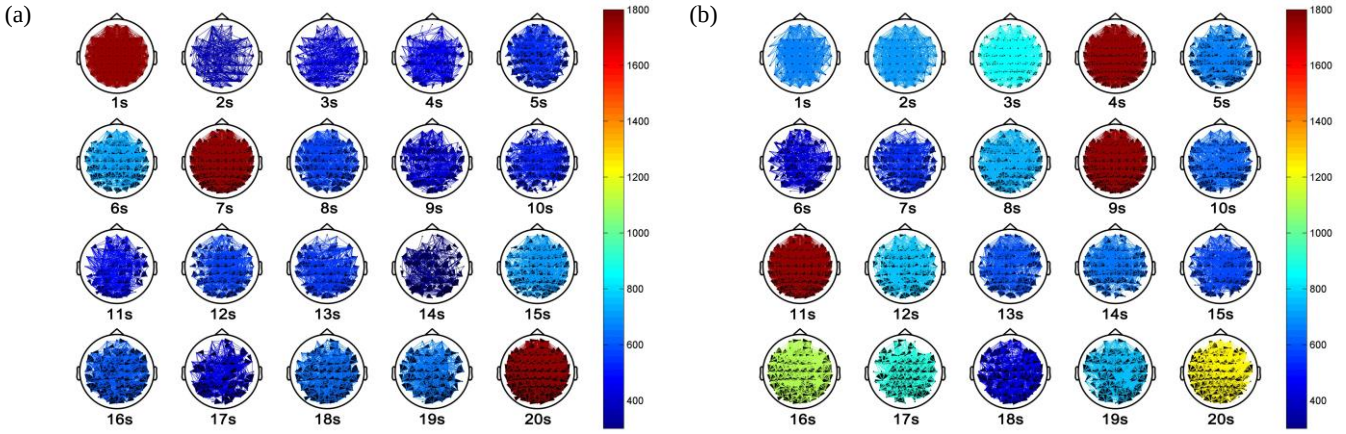

Fig. 13. Brain networks constructed by GC in the resting state. (a) Healthy control. (b) PI patient. Color bar indicates link number. The EEG electrodes were assigned to the nodes of the brain networks. The connectivity was estimated by GC and was binarized based on the adaptive threshold technology in Sec. 2.7. If there is a link between two nodes, it means the GC value exceeds the threshold *T*.

Fig. 14 shows the statistical analysis results of characteristics of brain networks constructed by GC. The blue and red lines represent the healthy control and PI groups respectively. All the characteristics present differentiation between groups. Most the averages of clustering coefficient and global efficiency of PI group are larger than those of healthy control group. On the contrary, most the averages of characteristic path length of PI group are shorter. Through unpaired two-sample *t*-test, it reveals statistically significant differences of clustering coefficient (p=0.0264), characteristic path length (p=0.0048), and global efficiency (p=0.0077) between groups.

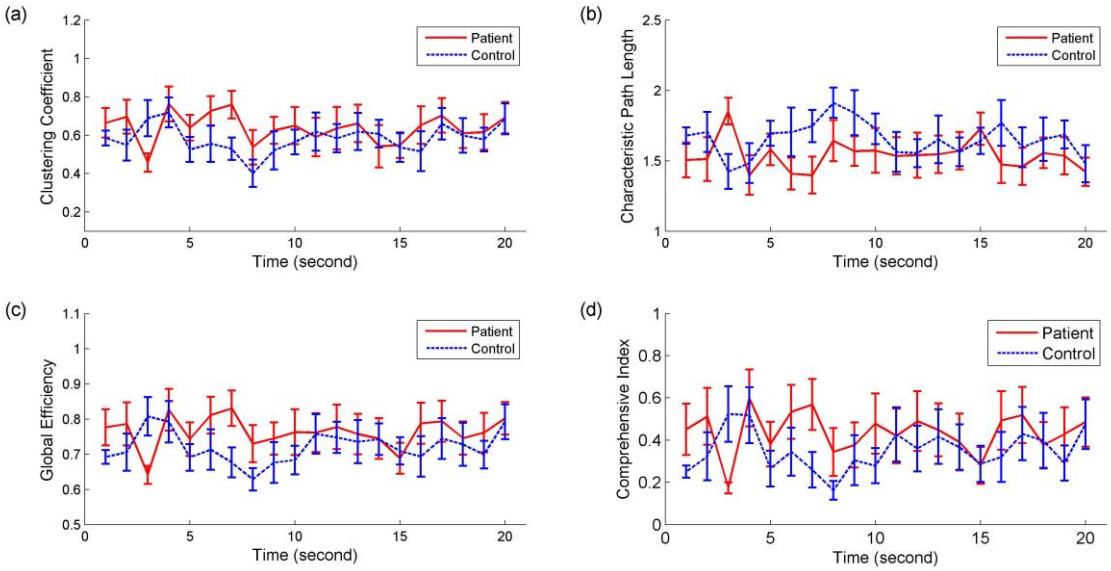

Fig. 14. Characteristics of brain networks constructed by GC in the resting state. (a) Clustering coefficient. (b) Characteristic path length. (c) Global efficiency. (d) Comprehensive index. Clustering coefficient C, characteristic path length L, global efficiency E_{global}, and comprehensive index η are calculated by Eqs. (15)-(18) respectively. Their averages and standard errors are plotted. The error bars are given in the form of mean ± standard deviation.

Fig. 14(d) shows the proposed comprehensive index of network characteristics under the condition of GC connectivity. The differentiation degree between groups is approximate to characteristic path length and global efficiency in Figs. 14(b) and (c). Most the comprehensive index averages of PI group are larger than those of healthy control group. Through unpaired two-sample *t*-test, it reveals statistically significant differences of comprehensive indices (p=0.0142**)** between groups**.** It indicates that the comprehensive index of PI group is significantly larger than that of healthy control group under the condition of PLI connectivity (p<0.05).

The comparison of the above network evaluation methods is presented in Table 3. Compared to the original network characteristics, the proposed comprehensive index can effectively distinguish PI and healthy control, no matter which connectivity estimation method was used. For the original network characteristics, the results of statistical analysis are different choosing different connectivity-estimated methods to construct brain networks. All of these network characteristics reveal significant differences between groups only when the connectivity was estimated by GC. It illustrates that it helps to improve the consistency of results when considering information flow based on the theory of causality.

Table 3. Brain network characteristics.

	Clustering Coefficient	Characteristic Path Length	Global Efficiency	Proposed Index
PCC	0.3938	**0.0015**	0.7042	**0.0021**
PLI	**0.0039**	0.0722	**0.0250**	**0.0071**
GC	**0.0264**	**0.0048**	**0.0077**	**0.0142**

Unpaired two-sample *t*-test is performed to compare the evaluation effects of different brain networks. *p* value in bold indicates significant difference between groups.

3.5. Classification based on brain network characteristics

Figs. 15 and 16 show the differences results of independent test set of four additional subjects. The number of connections for each network is indicated by the color within the color bar. As shown in Fig 15, the most PI's networks still have more links than the normal networks during the resting state of 20 seconds. The topological structure of the PI's networks is different from the healthy control. The dynamic regional blocks in Fig. 15 (a) are not observed in the PI's networks.

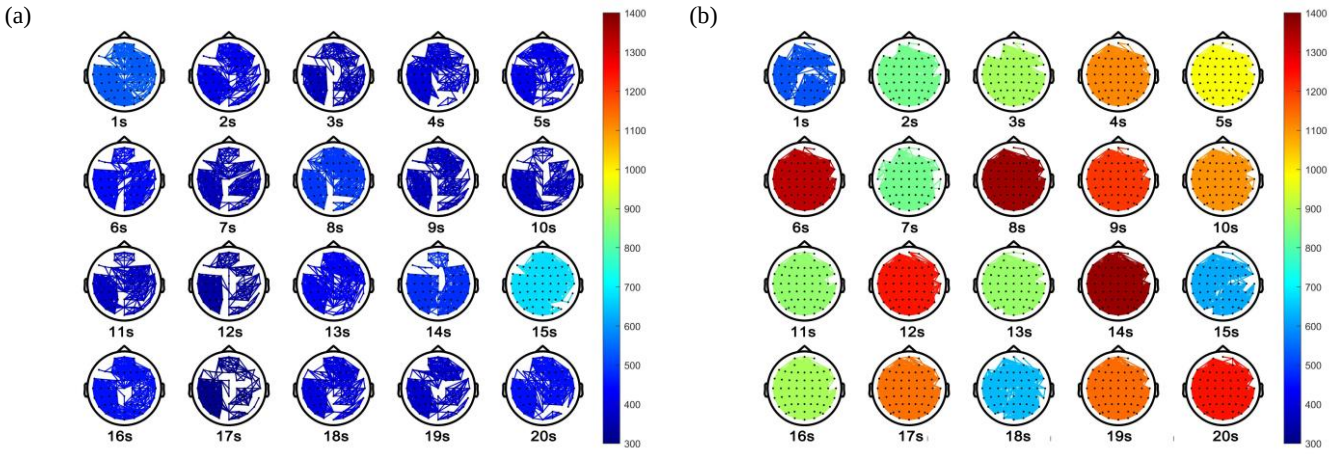

Fig. 15. Brain networks constructed by PCC in independent test set. (a) Normal individual. (b) PI patient. Color bar indicates link number. The EEG electrodes are assigned to the nodes of the brain networks. The connectivity is estimated by PCC and is binarized based on the adaptive threshold technology in Sec. 2.7. If there is a link between two nodes, it means the PCC value exceeds the threshold *T*.

Fig. 16 shows the characteristics of brain networks constructed by PCC. The blue and red lines represent the healthy and PI subjects respectively. They are distributed around different baselines. As shown in Fig. 16(d), the most points on the curves of the PI comprehensive index are above those of healthy subjects. It verifies that the comprehensive index of PI is bigger than that of healthy individual with fluctuations.

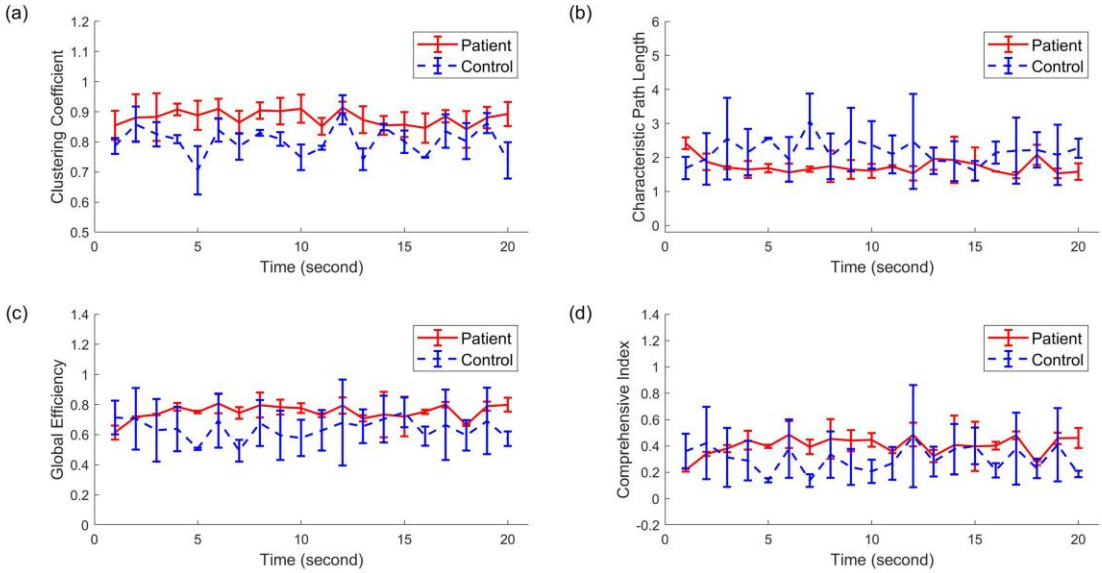

Fig. 16. Characteristics of brain networks constructed by PCC in independent test set. (a) Clustering coefficient. (b) Characteristic path length. (c) Global efficiency. (d) Comprehensive index. Clustering coefficient C, characteristic path length L, global efficiency E_{global}, and comprehensive index η are calculated by Eqs. (15)-(18) respectively. Their averages and standard errors are plotted. The error bars are given in the form of mean ± standard deviation.

The classification accuracy of the different network characteristics in the whole test set is presented in Table 4. It can be seen that the proposed comprehensive index achieves the best results. The accuracy and sensitivity of the proposed comprehensive index outperform the original network characteristics.

Table 4. Bi-LSTM classification results.

	Clustering Coefficient	Characteristic Path Length	Global Efficiency	Proposed Index
Accuracy (%)	35	80	60	**85**
Sensitivity (%)	40	80	20	**90**
Specificity (%)	30	80	100	**80**

The classification confusion matrices intuitively reflect the classification performance of the model for different classes of healthy status. Fig. 17 shows the confusion matrices in the whole test set trained by the different network characteristics. True label represents the actual healthy status. Predicted label represents the predicted healthy status of the classifier. Percentage indicates the output label ratio. Hence, the diagonal and non-diagonal lines respectively represent the classification accuracy and misclassification ratios of each status. The proposed comprehensive index has a high accuracy for two classes of healthy status (normal and PI), reaching 80% and 90%, respectively.

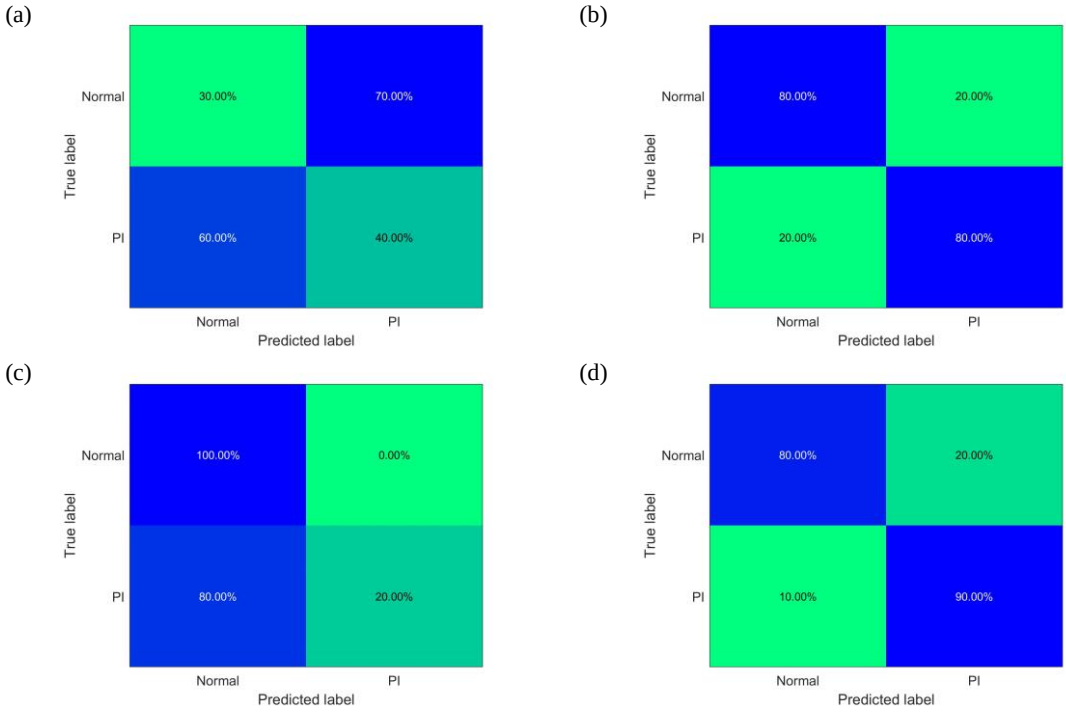

Fig. 17. Confusion matrices of classification in the whole test set. (a) Clustering coefficient. (b) Characteristic path length. (c) Global efficiency. (d) Comprehensive index. Clustering coefficient C, characteristic path length L, global efficiency E_{global}, and comprehensive index η are calculated by Eqs. (15)-(18) respectively. True label represents the actual healthy status. Predicted label represents the predicted healthy status of the classifier. Percentage indicates the output label ratio.

4. Discussion

According to some researchers, insomnia is closely related to high frequency power. The elevated Beta wave activity has been reported to be associated with high cortical arousal in PI patients [10, 11, 52, 53]. However, these studies focused on the EEG analysis of sleep stage. As argued by Corsi-Cabrera et al. [9], PI arousal effect also correlates with acquisition time and other factors. In this study, we did not get the result that the Beta power of PI was significantly higher than that of healthy control in the resting-state based on the traditional time-frequency analysis (see Fig. 8 and Table 2). From the perspective of isolated EEG activity in each brain area, the reason may be that the EEG data in this paper were all from the awake moment, and the brain was dominated by high frequency EEG activities such as Beta wave during this moment, which may lead to less obvious differences between the two groups. Although Beta power averages of the PI group in the specific channels are higher than those of the healthy control group (see Fig. 8) and the topographical distribution is different (see Fig. 7), no significant difference is revealed between group in the specific channels and localized sub-regions (frontal and posterior regions). Hence, PI may cause global disorder rather than just affecting local functional systems. Since the PI patients are often accompanied by the phenomenon of insufficient energy during the day [1], we believe the information of arousal effect is still involved in the PI group, but the time-frequency analysis implemented in each channel is not enough to reveal it. To extract and quantify the arousal features of PI, the connectivity was further estimated considering spatial interaction information.

Based on graph theory, PCC, PLI and GC were used to construct functional brain networks. They reflect spatial interaction information of different dimensions. As mentioned above, PCC represents an empirical characterization of the temporal relationship between regions. PLI is calculated from the asymmetry of the distribution of instantaneous signal phase differences between regions. GC embodies a spontaneous information flow and causal influence between regions. As shown in Figs. 9, 11, and 13, the brain networks of the PI and healthy individuals present differences of density and topology of connections under the three connectivity estimation methods. Overall, the PI networks have the denser links and their connectivity is stronger. Additionally, this visualized feature is relatively stable during the 20s resting state. Thus, these results are more reliable. They do not depend on the connectivity estimation methods.

The "small-world" measurements allow one to assess the robustness of topological features of the brain after undergoing trait- or state-like changes [53]. The common measures are clustering coefficient, characteristic path length, and global efficiency. In order to implement them and express the topology clearly, the networks need to be binarized. Only those elements of the adjacency matrix above a threshold indicate the existence of a connection between each pair of electrodes [14]. Obviously, the larger the threshold, the fewer the number of network connections and the fewer spurious edges. Nevertheless, when the threshold is too lager, isolated nodes will appear. There is no path to reach these nodes. The characteristic path length will be infinite. Therefore, choosing a reasonable threshold is crucial. In the this study, an adaptive threshold technology was introduced to conduct the binarization of brain networks. The threshold it determines is the maximum which makes the binarized networks belong to the connected graph. This minimize the number of spurious links while preventing the appearance of isolated nodes. Since the threshold is automatically determined, the data-driven method avoids the subjectivity and arbitrariness in manually selecting the threshold and facilitates the subsequent comparison of different network characteristics.

To quantitatively evaluate the global connectivity, the comprehensive index of network characteristics was calculated and compared with the original network characteristics. As shown in Figs. 10, 12, and 14, the proposed comprehensive index can distinguish between healthy control and PI groups, no matter which connectivity estimation method is used. The statistical analysis results revealed significant differences between groups under PCC (p=0.0021), PLI (p=0.0071), and GC (p=0.0142) conditions. In contrast, the results of the original network characteristics did not present statistical significance under every connectivity estimation condition, which might influence the result interpretation. Hence, the proposed comprehensive index has stronger generalization ability than the original network characteristics themselves.

The significantly larger comprehensive index of PI groups indicates strong "small-world" attributes of networks. It has bigger clustering coefficient, higher global efficiency, or shorter characteristic path length. It is believed that the small-worldness reflects the brain’s ability to efficiently integrate information [14]. Small world network is known as a network with high efficiency and low cost simultaneously. It has been proven that brain has a structure of small-worldness network, which makes it efficient in speedy information transmission [54]. The loss of "small-world" characteristics occur under conditions of reduced consciousness [55] and brain disorder like Alzheimer's disease [56-58]. Correspondingly, this paper shows that too strong "small-world" characteristics is also harmful and related to brain disorder. Obviously, the stronger "small-world" characteristics of PI do not represent the stronger brain’s ability than healthy control, but bring over-connectivity (see Figs. 9, 11, and 13). All the participants of PI group are recruited in the hospital. As recorded by PSQI and ISI, they are suffering from sleep disorders. Therefore, from another perspective, the results imply that the speedy information transmission of over-connectivity consumes more resources in the resting state. The brain with PI is difficult to achieve normal inhibition. This may be the cause of sleep disorders. Another asset that this paper brings is that the resting-state analysis is performed for the 20-second EEG. It exhibits a potential for rapid diagnosis in clinical practice. The network characteristics were input the Bi-LSTM classifier to judge the healthy status of a new subject automatically. As shown in Table 4 and Fig. 17, the classification accuracy of the proposed comprehensive index outperforms the original network characteristics. It is consistent with the evaluation performance of the proposed index. The PI patients’ index is higher than health controls with statistical significance (p<0.05). The proposed comprehensive index has a high accuracy for two classes of healthy status (normal and PI), reaching 80% and 90%, respectively. The sensitivity is also 90%. It indicates the missed diagnosis rate is relatively low. Compared with the original network characteristics, the proposed index is more sensitive to PI information. The future work will focus on exploration of relevant large scale datasets and optimized deep learning model to realize more accurate and reliable diagnosis and judgment for the state of disease progression.

5. Conclusion

In this paper, we presented a EEG-based quantitative analysis method of whole-brain connectivity in the resting state. With the network establishment, adaptive threshold technology and comprehensive index, it was proved that the hyperarousal information of PI could be mined not only in the sleep stages, but also in the resting state. The comprehensive index showed more versatility and stability performance than the original network characteristics under the connectivity estimations from different dimensions (PCC, PLI, and GC). The "small-world" features of PI were significantly stronger than healthy control, consistent with the arousal effect found by the previous studies during sleep. The characterization and quantization of over-connectivity in the 20s resting state is helpful for PI rapid diagnosis.

Acknowledgments

We gratefully acknowledge the financial support from the National Natural Science Foundation of China (grant number: 61703069 and 62001312) and the Fundamental Research Funds for the Central Universities (grant number: DUT21GF301).

Conflicts of Interest: The authors declare no conflict of interest.

References

1. Qaseem, A.; Kansagara, D.; Forciea, M. A.; Cooke, M.; Denberg, T. D.; Clinical Guidelines Comm, A. Management of Chronic Insomnia Disorder in Adults: A Clinical Practice Guideline From the American College of Physicians. *Annals of Internal Medicine* **2016,** 165, 2, 125-133.
2. Hertenstein, E.; Feige, B.; Gmeiner, T.; Kienzler, C.; Spiegelhalder, K.; Johann, A.; Jansson-Froejmark, M.; Palagini, L.; Ruecker, G.; Riemann, D.; Baglioni, C. Insomnia as a predictor of mental disorders: A systematic review and meta-analysis. *Sleep Medicine Reviews* **2019,** 43, 96-105.
3. Zhang, J.; Ma, R. C. W.; Kong, A. P. S.; So, W. Y.; Li, A. M.; Lam, S. P.; Li, S. X.; Yu, M. W. M.; Ho, C. S.; Chan, M. H. M.; Zhang, B.; Wing, Y. K. Relationship of Sleep Quantity and Quality with 24-Hour Urinary Catecholamines and Salivary Awakening Cortisol in Healthy Middle-Aged Adults. *Sleep* **2011,** 34, 2, 225-233.
4. Perlis, M. L.; Merica, H.; Smith, M. T.; Giles, D. E. Beta EEG activity and insomnia. *Sleep Medicine Reviews* **2001,** 5, 5, 365-376.
5. Merica, H.; Blois, R.; Gaillard, J. M. Spectral characteristics of sleep EEG in chronic insomnia. *European Journal of Neuroscience* **1998,** 10, 5, 1826-1834.
6. Kwan, Y.; Baek, C.; Chung, S.; Kim, T. H.; Choi, S. Resting-state quantitative EEG characteristics of insomniac patients with depression. *International Journal of Psychophysiology* **2018,** 124, 26-32.
7. Li, C.; Xia, L.; Ma, J.; Li, S.; Liang, S.; Ma, X.; Wang, T.; Li, M.; Wen, H.; Jiang, G. Dynamic functional abnormalities in generalized anxiety disorders and their increased network segregation of a hyperarousal brain state modulated by insomnia. *Journal of Affective Disorders* **2019,** 246, 338-345.
8. Zhao, W.; Van Someren, E. J. W.; Li, C.; Chen, X.; Gui, W.; Tian, Y.; Liu, Y.; Lei, X. EEG spectral analysis in insomnia disorder: A systematic review and meta-analysis. *Sleep medicine reviews* **2021,** 59, 101457-101457.
9. Corsi-Cabrera, M.; Rojas-Ramos, O. A.; del Río-Portilla, Y. Waking EEG signs of non-restoring sleep in primary insomnia patients. *Clinical Neurophysiology* **2016,** 127, 3, 1813-1821.
10. Spiegelhalder, K.; Regen, W.; Feige, B.; Holz, J.; Piosczyk, H.; Baglioni, C.; Riemann, D.; Nissen, C. Increased EEG sigma and beta power during NREM sleep in primary insomnia. *Biological Psychology* **2012,** 91, 3, 329-333.
11. Freedman, R. R. EEG power spectra in sleep-onset insomnia. *Electroencephalography and Clinical Neurophysiology* **1986,** 63, 5, 408-413.
12. Perlis, M. L.; Kehr, E. L.; Smith, M. T.; Andrews, P. J.; Orff, H.; Giles, D. E. Temporal and stagewise distribution of high frequency EEC activity in patients with primary and secondary insomnia and in good sleeper controls. *Journal of Sleep Research* **2001,** 10, 2, 93-104.
13. Imperatori, C.; Farina, B.; Adenzato, M.; Valenti, E. M.; Murgia, C.; Della Marca, G.; Brunetti, R.; Fontana, E.; Ardito, R. B. Default mode network alterations in individuals with high-trait-anxiety: An EEG functional connectivity study. *Journal of Affective Disorders* **2019,** 246, 611-618.
14. Sun, Y.; Lim, J.; Kwok, K.; Bezerianos, A. Functional cortical connectivity analysis of mental fatigue unmasks hemispheric asymmetry and changes in small-world networks. *Brain and Cognition* **2014,** 85, 220-230.
15. Onias, H.; Viol, A.; Palhano-Fontes, F.; Andrade, K. C.; Sturzbecher, M.; Viswanathan, G.; de Araujo, D. B. Brain complex network analysis by means of resting state fMRI and graph analysis: Will it be helpful in clinical epilepsy? *Epilepsy & Behavior* **2014,** 38, 71-80.

16. Bortoletto, M.; Veniero, D.; Thut, G.; Miniussi, C. The contribution of TMS–EEG coregistration in the exploration of the human cortical connectome. *Neuroscience & Biobehavioral Reviews* **2015,** 49, 114-124.
17. Park, H.-J.; Friston, K. J. Structural and Functional Brain Networks: From Connections to Cognition. *Science* **2013,** 342, 6158, 1-8.
18. Driver, J.; Blankenburg, F.; Bestmann, S.; Vanduffel, W.; Ruff, C. C. Concurrent brain-stimulation and neuroimaging for studies of cognition. *Trends in Cognitive Sciences* **2009,** 13, 7, 319-327.
19. Sohrabpour, A.; Cai, Z.; Ye, S.; Brinkmann, B.; Worrell, G.; He, B. Noninvasive electromagnetic source imaging of spatiotemporally distributed epileptogenic brain sources. *Nature Communications* **2020,** 11, 1, 1-15.
20. Killgore, W. D. S.; Schwab, Z. J.; Kipman, M.; DelDonno, S. R.; Weber, M. Insomnia-related complaints correlate with functional connectivity between sensory-motor regions. *Neuroreport* **2013,** 24, 5, 233-240.
21. Chen, M. C.; Chang, C.; Glover, G. H.; Gotlib, I. H. Increased insula coactivation with salience networks in insomnia. *Biological Psychology* **2014,** 97, 1-8.
22. Wang, T.; Yan, J.; Li, S.; Zhan, W.; Ma, X.; Xia, L.; Li, M.; Lin, C.; Tian, J.; Li, C.; Jiang, G. Increased insular connectivity with emotional regions in primary insomnia patients: a resting-state fMRI study. *European Radiology* **2017,** 27, 9, 3703-3709.
23. Horstmann, M.-T.; Bialonski, S.; Noennig, N.; Mai, H.; Prusseit, J.; Wellmer, J.; Hinrichs, H.; Lehnertz, K. State dependent properties of epileptic brain networks: Comparative graph-theoretical analyses of simultaneously recorded EEG and MEG. *Clinical Neurophysiology* **2010,** 121, 2, 172-185.
24. Nolte, G.; Bai, O.; Wheaton, L.; Mari, Z.; Vorbach, S.; Hallett, M. Identifying true brain interaction from EEG data using the imaginary part of coherency. *Clinical Neurophysiology* **2004,** 115, 10, 2292-2307.
25. Stam, C. J.; Nolte, G.; Daffertshofer, A. Phase lag index: Assessment of functional connectivity from multi channel EEG and MEG with diminished bias from common sources. *Human Brain Mapping* **2007,** 28, 11, 1178-1193.
26. Palva, J. M.; Wang, S. H.; Palva, S.; Zhigalov, A.; Monto, S.; Brookes, M. J.; Schoffelen, J.-M.; Jerbi, K. Ghost interactions in MEG/EEG source space: A note of caution on inter-areal coupling measures. *Neuroimage* **2018,** 173, 632-643.
27. Yan, C.; He, Y. Driving and Driven Architectures of Directed Small-World Human Brain Functional Networks. *Plos One* **2011,** 6, 8, 1-16.
28. Friston, K. J. Learning and inference in the brain. *Neural Networks* **2003,** 16, 9, 1325-1352.
29. Salinas, E.; Sejnowski, T. J. Correlated neuronal activity and the flow of neural information. *Nature Reviews Neuroscience* **2001,** 2, 8, 539-550.
30. Wu, L.; Huang, M.; Zhou, F.; Zeng, X.; Gong, H. Distributed causality in resting-state network connectivity in the acute and remitting phases of RRMS. *Bmc Neuroscience* **2020,** 21, 1, 1-8.
31. Raichle, M. E.; MacLeod, A. M.; Snyder, A. Z.; Powers, W. J.; Gusnard, D. A.; Shulman, G. L. A default mode of brain function. *Proceedings of the National Academy of Sciences of the United States of America* **2001,** 98, 2, 676-682.
32. Ma, X.; Jiang, G.; Fu, S.; Fang, J.; Wu, Y.; Liu, M.; Xu, G.; Wang, T. Enhanced Network Efficiency of Functional Brain Network in Primary Insomnia Patients. *Frontiers in Psychiatry* **2018,** 9, 1-11.
33. Beattie, L.; Espie, C. A.; Kyle, S. D.; Biello, S. M. How are normal sleeping controls selected? A systematic review of cross-sectional insomnia studies and a standardized method to select healthy controls for sleep research. *Sleep Medicine* **2015,** 16, 6, 669-677.
34. Goldstein, M. R.; Turner, A. D.; Dawson, S. C.; Segal, Z. V.; Shapiro, S. L.; Wyatt, J. K.; Manber, R.; Sholtes, D.; Ong, J. C. Increased high-frequency NREM EEG power associated with mindfulness-based interventions for chronic insomnia: Preliminary findings from spectral analysis. *Journal of Psychosomatic Research* **2019,** 120, 12-19.
35. Gurudath, N.; Riley, H. B., Drowsy Driving Detection by EEG Analysis Using Wavelet Transform and K-Means Clustering. In *9th International Conference on Future Networks and Communications*, Shakshuki, E. M., Ed. 2014; Vol. 34, pp 400-409.
36. Kar, S.; Bhagat, M.; Routray, A. EEG signal analysis for the assessment and quantification of driver's fatigue. *Transportation Research Part F-Traffic Psychology and Behaviour* **2010,** 13, 5, 297-306.

37. Zhang, C.; Ma, J.; Zhao, J.; Liu, P.; Cong, F.; Liu, T.; Li, Y.; Sun, L.; Chang, R. Decoding Analysis of Alpha Oscillation Networks on Maintaining Driver Alertness. *Entropy* **2020,** 22, 7.
38. Zhang, C.; Sun, L.; Cong, F.; Kujala, T.; Ristaniemi, T.; Parviainen, T. Optimal imaging of multi-channel EEG features based on a novel clustering technique for driver fatigue detection. *Biomedical Signal Processing and Control* **2020,** 62.
39. Zhang, C.; Cong, F.; Kujala, T.; Liu, W.; Liu, J.; Parviainen, T.; Ristaniemi, T. Network Entropy for the Sequence Analysis of Functional Connectivity Graphs of the Brain. *Entropy* **2018,** 20, 5.
40. Zhang, G.; Zhang, C.; Cao, S.; Xia, X.; Tan, X.; Si, L.; Wang, C.; Wang, X.; Zhou, C.; Ristaniemi, T.; Cong, F. Multi-domain Features of the Non-phase-locked Component of Interest Extracted from ERP Data by Tensor Decomposition. *Brain Topography* **2020,** 33, 1, 37-47.
41. Granger, C. W. J. Investigating Causal Relations by Econometric Models and Cross-Spectral Methods. *Econometrica* **1969,** 37, 3, 424-438.
42. Barnett, L.; Seth, A. K. The MVGC multivariate Granger causality toolbox: A new approach to Granger-causal inference. *Journal of Neuroscience Methods* **2014,** 223, 50-68.
43. Shaw, L.; Mishra, S.; Routray, A., Generalised orthogonal partial directed coherence as a measure of neural information flow during meditation. In *Advancements of Medical Electronics*, Springer: Berlin, 2015; pp 137-148.
44. Huang, D.; Ren, A.; Shang, J.; Lei, Q.; Zhang, Y.; Yin, Z.; Li, J.; von Deneen, K. M.; Huang, L. Combining Partial Directed Coherence and Graph Theory to Analyse Effective Brain Networks of Different Mental Tasks. *Frontiers in Human Neuroscience* **2016,** 10, 1-11.
45. Schindler, K. A.; Bialonski, S.; Horstmann, M.-T.; Elger, C. E.; Lehnertz, K. Evolving functional network properties and synchronizability during human epileptic seizures. *Chaos* **2008,** 18, 3, 1-6.
46. Atay, F. M.; Biyikoglu, T. Graph operations and synchronization of complex networks. *Physical Review E* **2005,** 72, 1, 1-7.
47. Humphries, M. D.; Gurney, K. Network 'Small-World-Ness': A Quantitative Method for Determining Canonical Network Equivalence. *Plos One* **2008,** 3, 4, 1-10.
48. Tang, S.; Qing, P.; Ye, M.; Lei, X. In *Altered Small-world Brain Network in Sleep Deprivation*, 2016 International Conference on Mechanical, Control, Electric, Mechatronics, Information and Computer, 2016; Pandey, K. M.; Mustapha, F., Eds. DEStech Publications, Inc.: 2016; pp 38-44.
49. Liao, X.; Vasilakos, A. V.; He, Y. Small-world human brain networks: Perspectives and challenges. *Neuroscience and Biobehavioral Reviews* **2017,** 77, 286-300.
50. Hu, X.; Yuan, S.l Xu, F. Scalp EEG classification using deep Bi-LSTM network for seizure detection. *Computers in Biology and Medicine* **2020,** 124, 103919.
51. Zheng, X.; Chen, W. An Attention-based Bi-LSTM Method for Visual Object Classification via EEG. *Biomedical Signal Processing and Control* **2021,** 63, 102174.
52. Meme, Y.; Pietrone, R.; Cashmere, J. D.; Begley, A.; Miewald, J. M.; Germain, A.; Buysse, D. J. EEG Power During Waking and NREM Sleep in Primary Insomnia. *Journal of Clinical Sleep Medicine* **2013,** 9, 10, 1031-1037.
53. Riemann, D.; Spiegelhalder, K.; Feige, B.; Voderholzer, U.; Berger, M.; Perlis, M.; Nissen, C. The hyperarousal model of insomnia: A review of the concept and its evidence. *Sleep Medicine Reviews* **2010,** 14, 1, 19-31.
54. Ahmadlou, M.; Adeli, H. Functional community analysis of brain: A new approach for EEG-based investigation of the brain pathology. *Neuroimage* **2011,** 58, 2, 401-408.
55. Uehara, T.; Yamasaki, T.; Okamoto, T.; Koike, T.; Kan, S.; Miyauchi, S.; Kira, J.-i.; Tobimatsu, S. Efficiency of a "Small-World" Brain Network Depends on Consciousness Level: A Resting-State fMRI Study. *Cerebral Cortex* **2014,** 24, 6, 1529-1539.
56. Micheloyannis, S.; Pachou, E.; Stam, C. J.; Breakspear, M.; Bitsios, P.; Vourkas, M.; Erimaki, S.; Zervakis, M. Small-world networks and disturbed functional connectivity in schizophrenia. *Schizophrenia Research* **2006,** 87, 1-3, 60-66.

57. Stam, C. J.; de Haan, W.; Daffertshofer, A.; Jones, B. F.; Manshanden, I.; van Walsum, A. M. v. C.; Montez, T.; Verbunt, J. P. A.; de Munck, J. C.; van Dijk, B. W.; Berendse, H. W.; Scheltens, P. Graph theoretical analysis of magnetoencephalographic functional connectivity in Alzheimers disease. *Brain* **2009,** 132, 213-224.

58. Stam, C. J.; Jones, B. F.; Nolte, G.; Breakspear, M.; Scheltens, P. Small-world networks and functional connectivity in Alzheimer's disease. *Cerebral Cortex* **2007,** 17, 1, 92-99.